From salinity to nanoplastics: redefining safe yield in strip-island aquifers under emerging contaminant threats

Tianyuan Zheng[1,2,3]*, Chunxiang Ma[1,2,3], Shaobo Gao[1,2,3], Jian Luo[4]**

[1] College of Environmental Science and Engineering, Ocean University of China, Qingdao, China, Qingdao 266100, China.

[2] Key Laboratory of Marine Environment and Ecology, Ministry of Education, Ocean University of China, Qingdao 266100, China.

[3] Shandong Provincial Key Laboratory of Marine Engineering Geology and the Environment, Ocean University of China, Qingdao 266100, China.

[4] School of Civil and Environmental Engineering, Georgia Institute of Technology, Atlanta, GA 30332, USA.

Corresponding authors: Tianyuan Zheng (zhengtianyuan@ouc.edu.cn);

Shaobo Gao (gaoshaobo@ouc.edu.cn)

Abstract: Nanoplastic contamination is emerging as a significant threat to groundwater security on small islands, where freshwater lenses serve as primary water supplies. Existing groundwater management frameworks are largely based on salinity intrusion and do not account for the distinct transport behavior of nanoplastics. This study formulates a multi-physics numerical model incorporating variable-density groundwater flow, salt transport, and nanoplastic migration processes to investigate nanoplastic transport in idealized strip-island aquifers under pumping conditions. The model is calibrated using laboratory-scale data and evaluated at the field scale. Results show that nanoplastic migration is controlled not only by advection – dispersion processes but also by particle-specific interactions, leading to transport dynamics fundamentally different from those of dissolved salts. In particular, the higher effective dispersivity of nanoplastics causes earlier breakthrough at extraction wells and the formation of broader contaminant transition zones. Pronounced scale effects are observed: while laboratory simulations exhibit rapid upward coning and contamination, field-scale simulations indicate attenuated coning and stabilization over substantially longer timeframes. Sensitivity analysis identifies nanoplastic dispersivity as the dominant parameter influencing well contamination risk. These findings demonstrate that safe extraction strategies based solely on salinity thresholds may underestimate contamination risks and that well placement and pumping design must account for nanoplastic transition zones. The study provides a process-based framework for adapting groundwater management to emerging nanoplastic pollution in vulnerable island environments.

Keywords: Groundwater lens; Seawater intrusion; Groundwater contamination; Pumping optimization

1. Introduction

Islands host nearly 10% of the global population and cover approximately 6.7% of the Earth's terrestrial surface (Sayre et al., 2019). On many small islands, limited surface water availability makes groundwater a critical resource for local communities (Dose et al., 2014). Notably, numerous Pacific islands rely on shallow freshwater lenses—buoyant bodies of freshwater overlying saltwater in highly permeable aquifers—as their primary water supply (Sharan et al., 2021; White and Falkland, 2010). The formation, stability, and morphology of these lenses result from the interplay between density contrasts and multiple external factors, including climate, geological structures, and anthropogenic activities such as groundwater pumping and subsurface barrier installation (Alsumaiei and Bailey, 2018; Ketabchi et al., 2014; Tang et al., 2021, 2022; Yan et al., 2021; Yang et al., 2025; Gao et al., 2025; Zheng et al., 2025). Excessive pumping readily induces saline upconing, degrades water quality, and threatens long-term water security (Abdoulhalik and Ahmed, 2018; Dagan and Bear, 1968; Houben and Post, 2017; Werner et al., 2009).

Beyond salinity intrusion, nanoplastic contamination has emerged as an additional and largely unaddressed threat to island groundwater systems. Microplastics are pervasive environmental pollutants detected in marine environments, soils, and groundwater worldwide (Koelmans et al., 2022; Koutnik et al., 2021; Li et al., 2018; Ren et al., 2021; Thompson et al., 2024). Oceanic concentrations continue to rise due to plastic persistence and ongoing inputs (Isobe et al., 2019). Nanoplastics, which are generated through the fragmentation of larger plastic debris and microplastics, may occur at even higher particle-number concentrations, with coastal waters often exhibiting higher levels than open-ocean regions (ten Hietbrink et al., 2025). Emerging evidence indicates that seawater intrusion facilitates the transport of microplastics into coastal aquifer systems (Chen et al., 2024). Because island aquifers are completely surrounded by seawater, freshwater lenses are particularly vulnerable to marine-sourced nanoplastic contamination (Fig. 1).

The maximum safe extraction rate for freshwater lenses is typically estimated

using analytical solutions that assume a sharp interface between freshwater and seawater (Muskat, 1938). Such approaches are widely used in two-dimensional strip-island models to determine the pumping threshold at which the saline interface reaches the well screen (Tang et al., 2020, 2021, 2024). While computationally efficient, these models neglect hydrodynamic dispersion and the development of a brackish transition zone, which can be extensive in highly permeable island aquifers (Coulon et al., 2022; Babu et al., 2020). Consequently, current safe-yield assessments often overlook realistic mixing processes and contaminant transport within the transition zone, potentially underestimating water-quality risks.

Transport processes of nanoplastics in porous media differ fundamentally from those of dissolved solutes. Early modeling efforts adapted classical advection-dispersion equations with simple adsorption terms (Babakhani et al., 2017), but subsequent studies have demonstrated that the migration of microplastics and nanoplastics involves additional mechanisms such as adsorption-desorption, clogging, interception, and aggregation (Liu et al., 2025; Yuan et al., 2024). Importantly, nanoplastic dispersion coefficients depend on particle size and flow velocity (Wang and Sedighi, 2023). Under pumping conditions that induce upward coning flow fields, these properties suggest that nanoplastics may migrate toward extraction wells more rapidly than dissolved salts and form a broader or earlier contaminant transition zone (Wang and Sedighi, 2023; Alkindi et al., 2011; Lee et al., 2017). Traditional sharp-interface and salinity-based intrusion models fail to capture this behavior, which has remained largely unexplored in island freshwater lens studies.

Taken together, there are two critical gaps that are interdependent and collectively undermine reliable groundwater management. First, existing safe-yield models oversimplify the freshwater-seawater transition zone by neglecting dispersion-driven mixing. This oversimplification is further exacerbated when combined with the poorly characterized transport of nanoplastics, which exhibit unique migration dynamics that cannot be captured by traditional solute models. Second, the distinct migration behavior of nanoplastics under pumping-induced

coning remains poorly understood. Current modeling frameworks, largely derived from solute transport theory, do not adequately capture transient nanoplastic breakthrough or particle-specific transport dynamics.

To address these gaps, this study develops a coupled numerical model that integrates variable-density groundwater flow, salt transport, and nanoplastic migration in island aquifers. This study aims to: (1) quantify marine-derived nanoplastic accumulation in freshwater extraction wells under pumping conditions; (2) assess how nanoplastic transport, especially enhanced dispersivity, alters the maximum safe extraction rate compared to traditional salinity-based thresholds; and (3) evaluate the sensitivity of nanoplastic migration and associated risks to key hydrogeological parameters and operational factors. By incorporating nanoplastic transport parameters derived from laboratory column experiments and conducting simulations at both laboratory and field scales, this work provides critical insights for adjusting groundwater management strategies to safeguard island freshwater resources in the face of emerging nanoplastic pollution.

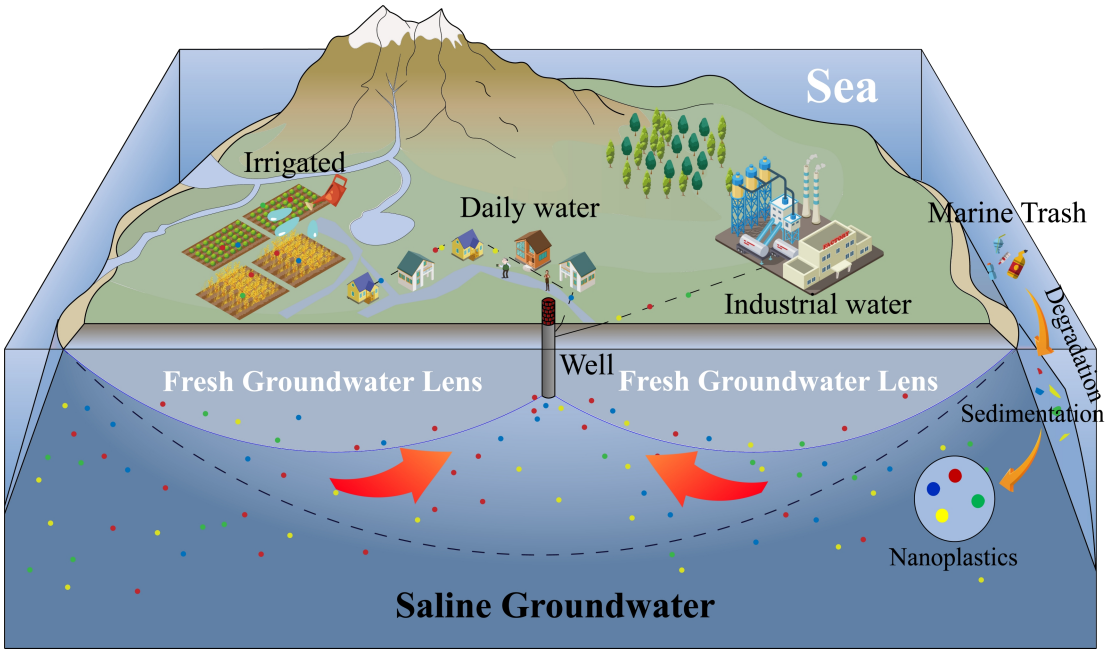

Fig. 1. Schematic diagram of freshwater lenses and nanoplastic contaminant distribution in an idealized strip-island aquifer under groundwater extraction.

2. Methods

2.1 Mathematical model

To simplify the problem and enhance computational tractability, the following key assumptions are adopted based on established modeling practices in coastal aquifer studies (Stoeckl and Houben, 2012; Yao et al., 2019): (i) the aquifer is homogeneous and isotropic; (ii) fluid density depends solely on groundwater salinity, with thermal effects considered negligible; (iii) the density of nanoplastic particles is assumed to be approximately equal to that of water, which is representative of neutrally buoyant or aged nanoplastic particles; (iv) the saturated zone is initially saturated with seawater, and rainfall infiltration is spatially uniform and temporally constant; (v) groundwater flow is simulated within a two-dimensional vertical profile of the strip island, leveraging the geometric symmetry of the idealized domain; and (vi) tidal influences are neglected, and constant head boundary conditions are imposed at the seawater interface.

This study presents an integrated numerical framework that extends a variable-density groundwater flow model for the unsaturated-saturated zone by incorporating salinity and nanoplastic transport modules. The nanoplastic transport model combines advective–dispersive transport with nanoplastic adsorption mechanisms. The resulting framework simultaneously simulates variable-density groundwater flow, dissolved salt transport, and nanoplastic migration via coupled advection-dispersion and adsorption processes. Governing equations for the variable-density flow and salinity transport components are available in Text S1.

Research suggests that nanoplastic transport is primarily influenced by particle movement and physical/physicochemical interactions with porous media surfaces (Al Harraq and Bharti, 2022; Ranjan et al., 2023; Ren et al., 2022; Waldschläger and Schüttrumpf, 2020). Particle movement is described in the equations as advection, diffusion and dispersion effects, while physicochemical interactions with porous media are characterized by mechanisms such as adhesion and detachment, straining on aggregates and individual particles, blockage, and maturation. The subsurface

transport of nanoplastic particles is governed by an advection-dispersion equation, a framework established for nanoplastic migration that captures advection, dispersion, and adsorption processes (Liu et al., 2025):

$$\frac{\partial}{\partial t}\left(S_{\mathrm{W}}\theta C_{\mathrm{np}}\right)+\frac{\partial}{\partial t}\left(\rho_{\mathrm{b}}s\right)+\nabla C_{\mathrm{np}}\frac{k_{\mathrm{r}}\mathbf{k}}{\mu}\nabla P+\nabla\cdot\left[-\theta S_{\mathrm{W}}D_{\mathrm{np}}\nabla C_{\mathrm{np}}\right]=f \tag{1}$$

$$\frac{\rho_{\mathrm{b}}\partial s}{\partial t}=\theta K_{\mathrm{att}}\psi_{\mathrm{b}}C_{\mathrm{np}}e^{-\frac{s}{\lambda}}-\rho_{\mathrm{b}}K_{\mathrm{det}}s+\theta\rho_{\mathrm{b}}K_{\mathrm{rip}}sC_{\mathrm{np}} \tag{2}$$

where C_{np} represents the concentration of nanoplastics in groundwater [$\mathrm{ML^{-3}}$], ρ_{b} denotes the bulk density of the aquifer medium [$\mathrm{ML^{-3}}$], s is the mass of nanoplastics attached per unit mass of solid [$\mathrm{MM^{-1}}$], D_{np} is the hydrodynamic dispersion coefficient of nanoplastics [$\mathrm{L^2T^{-1}}$], and f is the source-sink term [$\mathrm{ML^{-3}T^{-1}}$]. K_{att} is the first-order colloidal attachment coefficient [$\mathrm{T^{-1}}$], parameter λ represents the strain capacity of porous media [$\mathrm{MM^{-1}}$], K_{det} is the first-order colloidal detachment coefficient [$\mathrm{T^{-1}}$], and K_{rip} is the ripening kinetic rate coefficient [$\mathrm{M^{-1}L^3T^{-1}}$].

The adhesion of nanoplastics in porous media is described by the following governing equation:

$$\psi_{\mathrm{b}}=(1-\frac{s}{s_{\max}}) \tag{3}$$

where ψ_{b} denotes the adhesion state of nanoplastics in porous media [-], and $s_{\max}$ represents the maximum mass of nanoplastics that can be retained per unit mass of porous medium [$\mathrm{MM^{-1}}$].

The variation in hydraulic conductivity as a function of porosity is characterized by the following relationship (Zheng, 2014):

$$\frac{K}{K_0}=(\frac{\theta}{\theta_0})^3(\frac{1-\theta_0}{1-\theta})^3 \tag{4}$$

where K is the hydraulic conductivity of the porous medium [LT^{-1}], K_0 is the hydraulic conductivity of the initial porous medium [LT^{-1}], and θ_0 is the porosity of the initial water-bearing medium [-].

The approximate analytical solution derived by Tang et al. (2021) describes the critical pumping rate preventing brine intrusion when pumping wells are located in the idealized strip island's central region. The theoretical maximum safe extraction rate is expressed as:

$$Q_{\mathrm{Tmax}}=\omega\left(W-x_{\mathrm{m}}\right)-\frac{\delta(1+\delta)Kd^2}{\left(W-x_{\mathrm{m}}\right)} \tag{5}$$

$$\delta=\frac{\left(\rho_{\mathrm{s}}-\rho_{\mathrm{f}}\right)}{\rho_{\mathrm{f}}} \tag{6}$$

where ω is the infiltration rate at the upper surface of the unsaturated zone [LT^{-1}], ρ_s is the seawater density [ML^{-3}], ρ_f is the freshwater density [ML^{-3}], d is the distance from the well to the lower boundary of the unsaturated zone [L], W is the half width of the idealized strip island[L], x_m is the distance from the well to the centre of the idealized strip island[L].

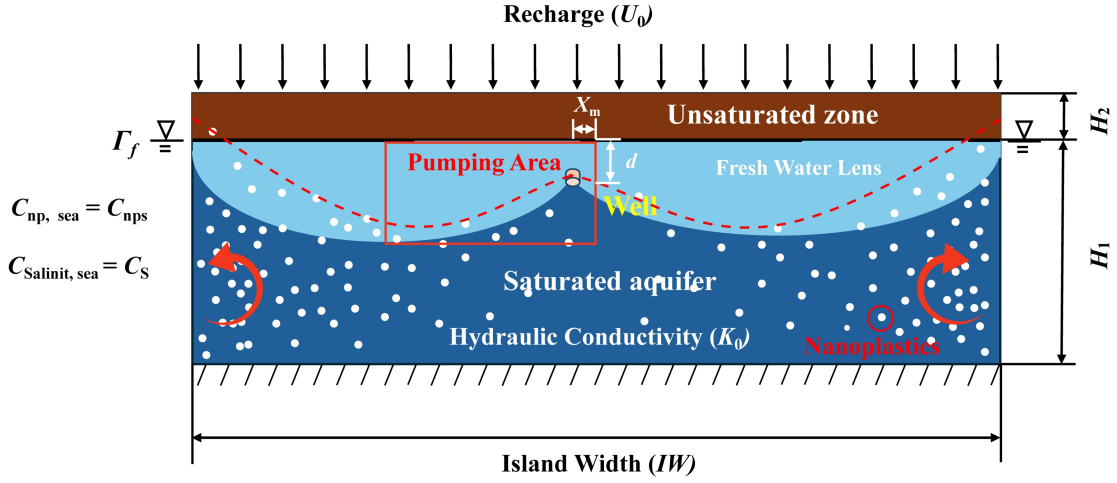

Fig. 2. Conceptual model of nanoplastic pollution in an idealized strip-island aquifer with central pumping. The model depicts an unsaturated zone (height H_2) over a saturated zone (height H_1). Freshwater lenses are shown in light blue and saline groundwater in dark blue. Key parameters include island width (IW), continuous recharge (U_0), seawater salinity (C_s), and seawater nanoplastic concentration (C_{nps}).

2.2 Numerical Solution

The numerical simulation investigates the migration behavior of nanoplastics under pumping conditions in an idealized strip-island aquifer. The laboratory-scale model domain (60 cm×17 cm) was constructed following the configuration established by Tang et al. (2021) (Fig. S4), while a field-scale model (600 m×50 m) was developed to assess field-level transport phenomena. Key simulation parameters are provided in Table 1. Model parameters calibrated from laboratory-scale experiments were extrapolated to the field scale assumed for the modeling study to evaluate the consistency of nanoplastic migration patterns across scales. At the ocean boundary, a constant head (Dirichlet) condition was imposed with a specified hydraulic head (H_1) and a salt concentration of 34.7 g/L; tidal influences were neglected. A constant flux (Neumann) condition was applied to the upper boundary, representing recharge at a rate U_0. Fig. 2 shows a vertical cross-section of a typical freshwater lens in an idealized island under single-well pumping conditions. Additional aquifer properties are summarized in Table 1.

Table 1. Numerical Simulation Parameters for Variable-Density Flow and Nanoplastic Transport (Laboratory and Field Scales)

Parameter	Symbol	Unit	Value
Variable density parameter			
Density of sea water	ρ_0	kg/m^3	1025
Density of freshwater	ρ_f	kg/m^3	1000
Seawater salinity	C_s	mol/L	0.5989

Nanoplastics properties PS-Pd-1			
Constant[a, b]	λ	mg/kg	1.6
First-order colloidal attachment coefficient[a, b]	K_{att}	1/s	0.0025
Euler number[a]	e	—	2.7183
The maximum solid phase particle concentration[a, b]	S_{max}	mg/kg	10
First-order colloidal detachment coefficient[a, b]	K_{det}	1/s	0.001
Ripening kinetic rate coefficient[a, b]	K_{rip}	m^3 /(g·s)	0.009
Longitudinal dispersivity[b]	$\alpha_{LPS-Pd-1}$	cm	0.91
The average relative molecular weight of nanoplastics[c]	N_m	g/mol	70000
Nanoplastics properties PS-Pd-2			
Constant[a, b]	λ	mg/kg	1.7
First-order colloidal attachment coefficient[a, b]	K_{att}	1/s	0.0002
The maximum solid phase particle concentration[a, b]	S_{max}	mg/kg	10
First-order colloidal detachment coefficient[a, b]	K_{det}	1/s	0.005
Ripening kinetic rate coefficient[a, b]	K_{rip}	m^3 /(g·s)	0.007
Longitudinal dispersivity[b]	$\alpha_{LPS-Pd-2}$	cm	1.06
The average relative molecular weight of nanoplastics[c]	N_m	g/mol	70000
Laboratory Porous medium properties			
Island width[d]	IW	cm	60
Saturated zone thickness[d]	H_1	cm	15

Unsaturated zone thickness[d]	H_2	cm	2
Rainfall infiltration[d]	U_0	cm/min	0.80
Porosity[d]	θ_0	—	0.38
Longitudinal dispersivity	α_L	cm	0.2
Hydraulic conductivity[d]	K_0	cm/min	200
Field-scale Porous medium properties			
Island width	IW	m	600
Saturated zone thickness	H_1	m	45
Unsaturated zone thickness	H_2	m	5
Rainfall infiltration	U_0	m/s	2×10^{-8}
Porosity	θ_0	—	0.38
Longitudinal dispersivity	α_L	m	0.5
Hydraulic conductivity	K_0	m/s	0.0001

a. Data from Liu et al. (2025)

b. Data inversion was performed based on the experimental data.

c. Data from Singh et al. (2025)

d. Experimental water pumping scenario from Tang et al. (2021)

The coupled governing equations for variable-density saturated groundwater flow and solute transport were solved numerically via COMSOL Multiphysics, with boundary conditions prescribed accordingly. The system of equations was solved iteratively using a preconditioned conjugate gradient (PCG) method with a relative tolerance of 1×10^{-4}. Initial time steps of 0.001 s and 0.001 d were adopted for the transient analyses.

The computational domain for the laboratory-scale model was discretized into 63,928 triangular elements and 32,350 nodes, with a maximum element diameter of 2 mm. For the field-scale model, the domain was discretized into 30,000 quadrilateral elements and 30,651 nodes, with a maximum element diameter of 1 m. The selected mesh sizes, in conjunction with the hydrodynamic dispersion parameters, conformed

to the Péclet number criterion to minimize numerical dispersion and ensure solution stability (Voss and Provost, 2002):

$$Pe_1 = \frac{v_1 \Delta L_1}{D_1 + \alpha_{L1} v_1} \approx \frac{\Delta L_1}{\alpha_{L1}} = 1 \leq 4 \tag{7}$$

$$Pe_2 = \frac{v_2 \Delta L_2}{D_2 + \alpha_{L2} v_2} \approx \frac{\Delta L_2}{\alpha_{L2}} = 2 \leq 4 \tag{8}$$

where Pe_1 is the Péclet number in laboratory-scale [-], Pe_2 is the Péclet number in field-scale [-], ΔL_1 is the grid length in laboratory-scale [L], ΔL_2 is the grid length in field-scale [L], v_1 is flow velocity in laboratory-scale [LT^{-1}], v_2 is flow velocity in field-scale [LT^{-1}], D_1 is diffusion coefficient in laboratory-scale [L^2T^{-1}], D_2 is diffusion coefficient in field-scale [L^2T^{-1}], α_{L1} is the longitudinal dispersivity in laboratory-scale [L], α_{L2} is the Longitudinal dispersivity in field-scale [L].

Stabilization times for laboratory and field simulations were determined using a convergence criterion: the system was considered stable when the relative change in wellhead salinity and nanoplastic concentration was less than 1% over three consecutive time steps.

A continuous rainfall-driven model was developed to simulate freshwater lens dynamics and well extraction in an idealized island aquifer. The simulation comprises two distinct hydraulic phases: Phase I involves the formation of a stable freshwater lens under continuous rainfall infiltration and seawater intrusion; Phase II initiates groundwater extraction via a single pumping well, leading to the development of a stable saline upconing zone. In the laboratory-scale setup, the horizontal distance x_m from the pumping well to the island center was set to 0, 2.5, 5, 7.5, 10, 12.5, 15, 17.5, and 20 cm. The vertical distance d from the well screen to the base of the saturation zone was defined as 0, 5, 10, 12, 15, 18, 20, and 25 mm. Hydraulic conductivity K_0 values were assigned as 150, 175, 200, 225, and 250 cm/min, with corresponding

recharge rates U_0 of 0.6, 0.7, 0.8, 0.9, and 1.0 cm/min. For the field-scale scenario, the pumping well was positioned at a horizontal distance x_m=5 m from the island center, corresponding to a central well location. The hydraulic conductivity K_0 was set to 1×10^{-4} m/s, with a recharge rate $U_0 = 2\times10^{-8}$ m/s (Tang et al., 2021).

2.3 Evaluation Indicators

Nanoplastic concentrations at the wellhead were monitored to evaluate the impacts of nanoplastics on island freshwater lens development projects. The seawater-freshwater interface of the freshwater lens was designated as 0.347 g/L, corresponding to 1% seawater salinity. Contemporary laboratory investigations typically utilize nanoplastic concentrations ranging from 10 μg/L to 100 mg/L. Owing to constraints associated with nanoplastic preparation protocols and detection capabilities, the migration parameters of nanoplastics in this study were derived under an initial concentration of 10 mg/L. Nanoplastics at 100–500 μg/L can exert widespread toxicity to marine organisms including bivalves, sea urchins, algae, and bacteria (Gonçalves and Bebianno, 2021). Adopting the 1% seawater salinity threshold as a reference for nanoplastic concentrations facilitates comparisons of migration patterns between nanoplastics and dissolved salts under freshwater extraction scenarios in idealized strip-shaped islands, while incorporating the biological toxicity of nanoplastics as a critical constraint.

Concurrently, the distribution of nanoplastics within freshwater lenses is characterized by comparing the volume reduction rate (VR) of freshwater lenses over a given time period:

$$VR = \frac{V_0 - V_w}{V_0} \tag{9}$$

where V_w represents the volume of freshwater lenses surrounded by nanoplastics pollution [L^3], V_0 represents the volume of freshwater lenses surrounded by saline water [L^3].

Accounting for the implications of the transition zone theory for groundwater pumping practices, the following indicator is defined: the ratio of the actual maximum safe extraction capacity to the theoretical maximum safe extraction capacity (*ASYR*):

$$ASYR = \frac{Q_{\mathrm{Amax}}}{Q_{\mathrm{Tmax}}} \tag{10}$$

where Q_{Amax} represents the actual maximum safe extraction volume [L^3T^{-1}], Q_{Tmax} represents the theoretical maximum safe extraction volume [L^3T^{-1}]

Taking into account the potential reduction in groundwater extraction capacity induced by nanoplastic contamination, the following indicator is defined: the ratio of the maximum safe extraction capacity reduction caused by nanoplastic retention to the maximum safe extraction capacity (*RRSY*):

$$RRSY = \frac{Q_{\mathrm{Amax}} - Q_{\mathrm{Smax}}}{Q_{\mathrm{Amax}}} \tag{11}$$

where Q_{Smax} represents the maximum safe extraction volume without nanoplastic influence [L^3T^{-1}].

Table 2 provides a systematic description of the representative roles of the three evaluation metrics used in this paper:

Table 2. Summary of Evaluation Indicators and Their Functions

Symbol	Full name	Description
VR	Volume reduction rate	Quantifies the shrinkage degree of usable freshwater lens volume under nanoplastic contamination.
ASYR	Ratio of the actual maximum safe extraction capacity to the theoretical	Evaluates the reduction degree of practical safe extraction capacity relative to the theoretical threshold.

	maximum safe extraction capacity	
RRSY	Ratio of the maximum safe extraction capacity reduction caused by nanoplastic retention to the maximum safe extraction capacity	Assesses the additional loss of safe extraction capacity specifically caused by nanoplastic retention and contamination.

2.4 Model Calibration

This study examined the migration patterns of two synthetic nanoplastics (PS-Pd-1 and PS-Pd-2) that exhibit contrasting hydrophobicity. The detailed synthesis protocols are available in Supplementary Materials (Text S2). To ensure model accuracy, migration parameters for nanoplastics in quartz sand (Table 1) were validated using column experiment data from Liu et al. (2025). The experimental setup and methodology are detailed in Text S3 and Fig. S1, with calibration processes and results illustrated in Fig. S2 and S3. The primary objective was to quantify how differential nanoplastic-solid phase interactions influence contamination levels in freshwater lenses (Amirmoshiri et al., 2020; Wang et al., 2021). As summarized in Table 1, PS-Pd-1 exhibits strong solid-phase adsorption capacity, whereas PS-Pd-2 demonstrates weaker adsorption. Given potential scale-dependence in nanoplastic transport parameters, current research remains largely focused on laboratory-scale investigations (Johnson, 2020; Li et al., 2021; Liu et al., 2025).

A single-well extraction scheme was implemented in the central region of an idealized strip island aquifer. The maximum safe extraction rate, calculated based on sharp-interface theory, served as the baseline scenario. However, the applicability of this theoretical maximum for island freshwater lenses requires critical re-evaluation, as previous sharp-interface analytical and numerical studies have largely neglected the transition zone formed by salinity dispersion and diffusion—a factor addressed in

only limited corrections (Coulon et al., 2022). To determine a more accurate maximum safe extraction rate, a series of numerical simulations with predefined pumping rates were conducted to calibrate both laboratory-scale and field-scale conceptual models.

Although Tang et al. (2021) provided preliminary numerical validation via Fig. S4(a)(b), their simulations omitted the effects of the unsaturated zone and the salinity transition zone. In contrast, our validation-based simulations (Fig. S4(c)(d)), which incorporate the unsaturated zone and employ dispersion parameters consistent with Chen et al. (2024a), indicate that the 1% salinity contour exceeds the well bottom elevation by 2.03 m. This signifies that pumping-induced salinity surpasses regulatory thresholds, necessitating a reduction in extraction volume.

The relationship between well salinity and the extraction volume ratio (actual to theoretical) in numerical simulations is illustrated in Fig. 3. Results confirm that the presence of the unsaturated and transition zones reduces the extraction capacity to 50% – 60% of the theoretical maximum (Q_{Tmax}). Specifically, under laboratory conditions, the maximum safe extraction capacity decreased to 61% and 53% of Q_{Tmax} for shallow (d=0 cm) and deep (d=1.5 cm) extraction scenarios, respectively (Fig. 3(a)). Corresponding field-scale simulations showed reductions to 57% and 51% of Q_{Tmax} for shallow (d=0 m) and deep (d=15 m) extraction. The temporal evolution of well salinity during freshwater lens re-stabilization (Fig. 3(b)) further demonstrates that salinity stabilization occurs within 12 minutes at the laboratory scale but requires approximately 4.5 years at the field scale, highlighting significant temporal disparities influenced by scale effects.

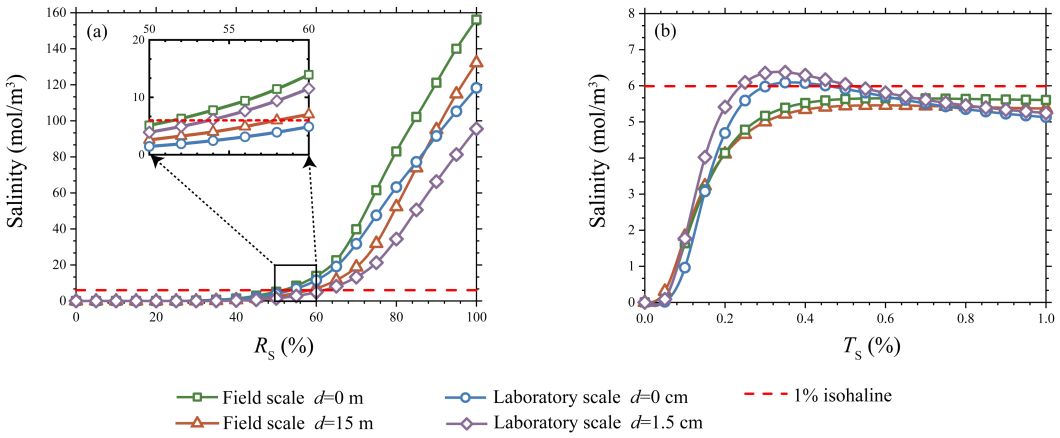

319

320 Fig. 3. Variations in well salinity as a function of the ratio of extraction volume to
321 theoretical maximum (R_S) and the ratio of time to theoretical equilibrium time (T_S)
322 during pumping at different depths in numerical simulations , measured at both field
323 and laboratory scales: (a) Well salinity versus extraction volume, with the magnified
324 region indicating the extraction volume range where well concentration approaches
325 the 1% isohaline; (b) Temporal concentration variations for wells with salinity near
326 the 1% isohaline in panel (a).

327 **3. Results and Discussion**

328 **3.1 Distribution Patterns of Nanoplastics Under Pumping Conditions**

329 Hydrophobic nanoplastics (NPs) were selected as the primary research focus of
330 this study. Text S4 and Fig. S5 demonstrate that hydrophobic nanoplastic particles
331 exhibit higher mobility and pose more significant hazards than hydrophilic
332 counterparts under simulated single-well pumping conditions.

333 Fig. 4(a_1-a_4) illustrates an "upper cone" phenomenon in nanoplastic
334 concentrations during pumping, analogous to that of salinity. Fig. 4(a_1) reveals that
335 highly dispersive nanoplastics may form anomalous distributions in the central
336 banded region of the island—a zone previously referred to as the "stagnation zone"
337 (Wang et al., 2023). Nearshore aquifers on both sides of the island undergo intense
338 convection, driven by groundwater discharge to the sea and seawater intrusion
339 induced by density currents. At the laboratory scale, this convective zone spans

approximately 10 cm; at the field scale, it extends to around 100 meters, where groundwater Darcy velocities exceed 1×10^{-3} m/s. In contrast, velocities within the central "stagnation zone" remain below 1×10^{-8} m/s. This zone is dominated by weak convection, with material transport in groundwater primarily governed by dispersion and interactions with the solid phase.

Fig. 4(b) presents dynamic nanoplastic isoconcentration lines at the wellhead, where concentrations first increase and then decrease—indicating that wellhead nanoplastics are influenced by the "stagnation zone". The discrepancy in migration behavior between nanoplastics and dissolved solutes stems primarily from their distinct physicochemical properties: as colloidal particles, nanoplastic migration is regulated not only by advection-dispersion but also by particle-medium interactions (e.g., adsorption-desorption, clogging, and filtration). Fig. 4(c_1-c_3) depicts variations in nanoplastic concentrations. Considering the nanoplastic concentration threshold resulted in an additional 37.48% reduction in the usable freshwater lens area, while the maximum depth of freshwater zones affected by nanoplastic contamination increased by 0.030 m.

Fig. 4(d_1-d_4) compares the distribution patterns of salinity and nanoplastics, revealing that nanoplastics exceeding 1% of the critical nanoplastic concentration (C_{nps}) are concentrated within freshwater lens layers. With the disappearance of the original "stagnation zone", a new flow field transition zone is formed, triggering the emergence of a new "stagnation zone". The proportion of the freshwater lens occupied by the nanoplastic transition zone (dark blue areas in Fig. 4(d_1-d_4)) increased from 30.27% to 41.24%. Compared to dissolved solutes, nanoplastics possess larger hydrodynamic diameters and unique surface properties, leading to distinctive migration patterns in porous media.

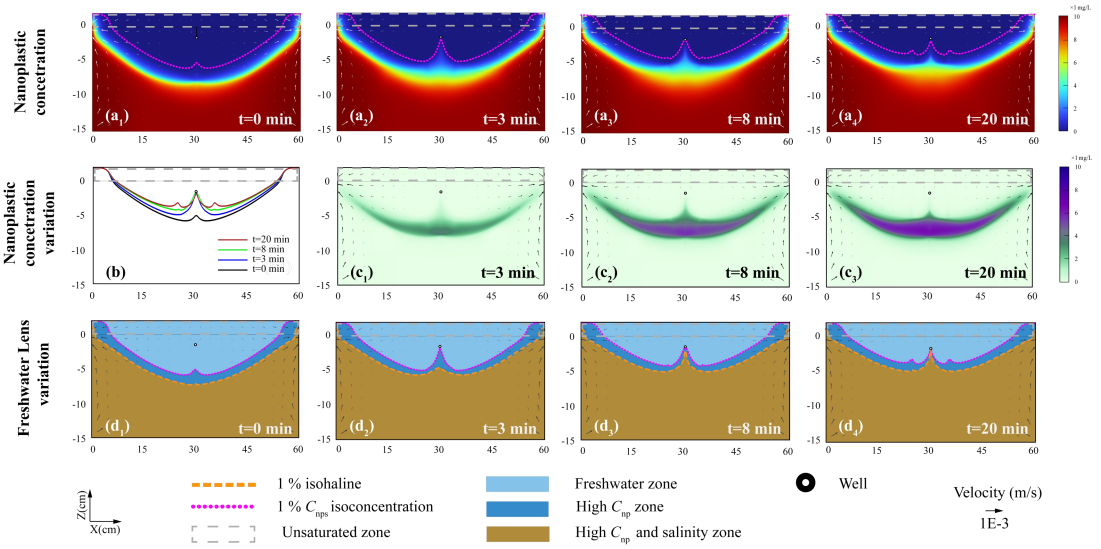

365

366 Fig. 4. Distribution and concentration dynamics of PS-Pd-2 hydrophobic nanoplastics
367 and corresponding freshwater lens alterations at the laboratory scale (60 cm×17 cm)
368 during pumping (R_S = 53%) in numerical simulations: (a_1-a_4) freshwater lenses
369 demarcated by the 1% isoconcentration line of PS-Pd-2 hydrophobic nanoplastics at 0,
370 3, 8 and 20 minutes post-pumping, (b) temporal variation of the 1% C_{nps}
371 isoconcentration line, (c_1-c_3) net concentration variations relative to the baseline (0
372 min) at 3, 8 and 20 minutes post-pumping, (d_1-d_4) spatial offset between the 1%
373 isohaline and 1% C_{nps} isoconcentration line around the freshwater lens.

374 Fig. 5(a) presents the vertical concentration profile of nanoplastics at the
375 wellhead, further validating the aforementioned mechanism. Prior to pumping
376 initiation, the nanoplastic transition zone was situated 0.07 - 0.10 m below the well
377 bottom. Following pumping initiation, the transition zone underwent a rapid upward
378 migration and expansion to 0.02 m below the well bottom. Thirty minutes
379 post-pumping, although the transition zone exhibited a slight recession, a stable
380 transition zone was maintained at 0.06 m below the well bottom, while a new steep
381 transition zone formed at 0.03 m. Nanoplastic concentrations at the wellhead
382 increased markedly within the first 4 minutes, started to decline after 8 minutes,
383 stabilized at 30 minutes post-pumping, and ultimately converged with the
384 concentration trends of chloride (Cl^-), indicating that solute and colloidal transport are

385 governed primarily by convection. The observed transport behavior can be interpreted
386 through the lens of effective dispersion parameters. In porous media transport
387 modeling, the macroscopic dispersion coefficient in advection-dispersion equations
388 serves as an effective parameter that implicitly captures the integrated effects of
389 various pore-scale processes, including particle-pore interactions, flow path tortuosity,
390 and temporary retention at pore throats. While these microscopic processes are not
391 explicitly resolved in the current continuum-scale model, their integrated effects are
392 reflected in the calibrated dispersion parameters.

393 Fig. 5(b) illustrates the temporal concentration variations of hydrophilic and
394 hydrophobic nanoplastics, both of which exhibit an initial increase followed by a
395 subsequent decrease. During the initial pumping phase (0 - 6 min), high-concentration
396 nanoplastics in the immediate vicinity of the well were the primary fraction extracted
397 by pumping, leading to a sharp concentration increase to a peak of 2.489% C_{nps}. With
398 prolonged pumping (6 - 32 min), peripheral groundwater with relatively low
399 nanoplastic concentrations gradually entered the pumping-affected zone. The original
400 stagnation zone was reconfigured under the influence of pumping, with new
401 stagnation zones emerging on both sides of the well. The system eventually attained a
402 state of dynamic equilibrium after 32 min of pumping, with nanoplastic
403 concentrations stabilizing at a steady level. Notably, salinity variations under distinct
404 contamination scenarios involving hydrophilic and hydrophobic nanoplastics also
405 influenced this process. This phenomenon is hypothesized to originate from an
406 approximate 40% reduction in hydraulic conductivity, which is induced by the
407 solid-phase enrichment of hydrophilic nanoplastics in specific central regions of the
408 study domain.

409 With respect to the distinct distribution characteristics of wellborne hydrophobic
410 nanoplastics presented in Fig. 5(b), which diverge from those of salinity, the
411 application of a 1% concentration threshold to nanoplastics (consistent with the
412 salinity threshold) results in wellhead nanoplastic concentrations exceeding this
413 criterion for more than 80% of the duration prior to the attainment of a stable system

state. To mitigate the adverse impacts of the extensive dispersion of hydrophobic nanoplastics on the quality of pumped groundwater, Fig. 5(c) shows the relationships between wellhead nanoplastic concentrations and cumulative pumped water volume for hydrophilic and hydrophobic nanoplastics. Under the theoretical maximum safe pumping rate, hydrophobic nanoplastics accumulate at the wellhead to a concentration of 1.939 mg/L during the initial pumping phase. To reduce the initial wellhead nanoplastic concentrations to below the 1% C_{nps} threshold, the actual maximum safe pumping rate must be further reduced to 37% of the theoretical maximum safe pumping rate. Fig. 5(d) indicates that a similar phenomenon is observable in wellhead nanoplastic concentrations at the field scale, where nanoplastics at such concentrations are still rapidly entrained into the pumping well—indicating that the enrichment mechanism driven by high nanoplastic dispersibility remains valid at the field scale. High-concentration nanoplastic influxes at the wellhead persisted from years 5 to 28 at the field scale. Conversely, nanoplastic concentrations in the upper cone region are comparatively lower, with those in the island’s pumping wells reaching only 1.329% C_{nps}. A detailed elucidation of the underlying mechanisms for this phenomenon is presented in Section 3.2.

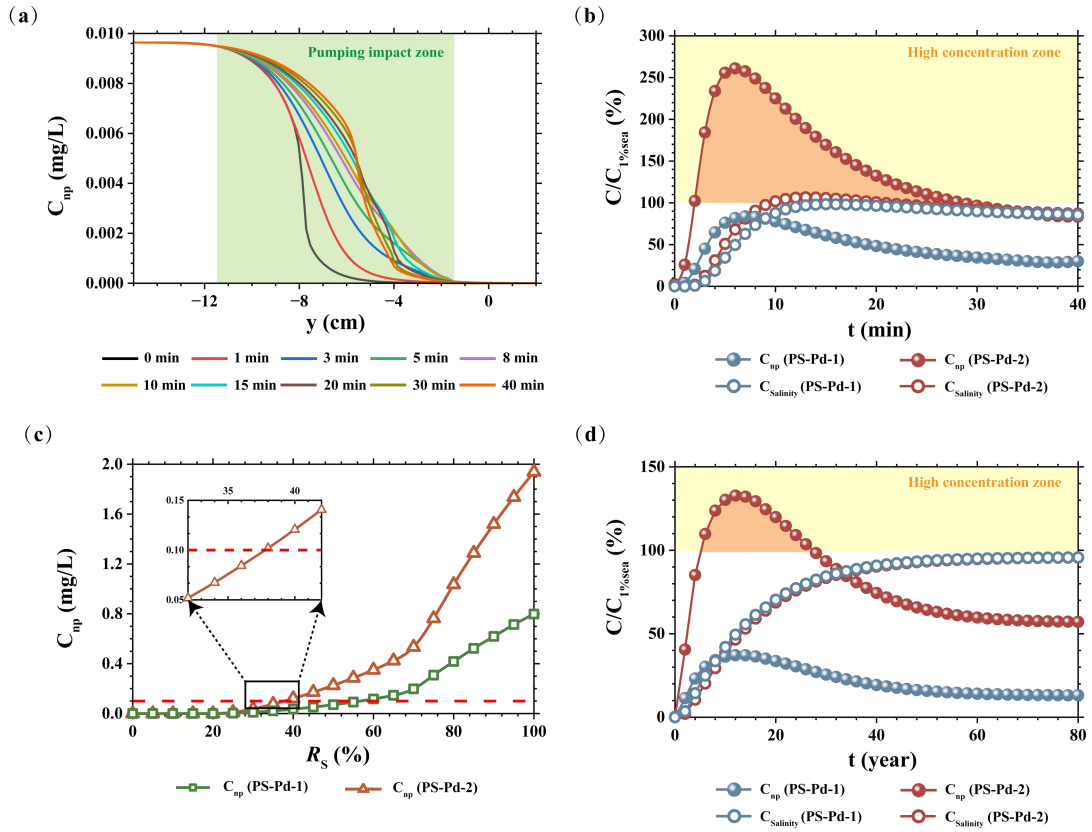

Fig. 5. Concentration dynamics at laboratory and field scales and their responses to pumping rate adjustments in numerical simulations: (a) 1% C_{nps} isoconcentration line variation along the central axis (x=30 cm) at laboratory scale; (b) Temporal variations in salinity and nanoplastic concentrations for hydrophilic and hydrophobic nanoplastics at laboratory scale; (c) Well nanoplastic concentration as a function of pumped volume-to-theoretical maximum ratio (R_S) for groundwater nanoplastics of distinct hydrophilic-hydrophobic properties; (d) Temporal variations in well salinity and nanoplastic concentrations for hydrophilic and hydrophobic nanoplastics at field scale.

3.2 Scale Effects on Nanoplastic Transport

In field-scale simulations, the background concentration of hydrophobic nanoplastics was set to 1 μg/L (C_{nps}). Dispersion parameters were adjusted based on scaling-up experience (Gelhar et al., 1992), with the corresponding simulation results presented in Fig. 6. Fig. 6(a_1) shows that following stabilization of the freshwater lens, the 90%–10% C_{nps} transition zone in the central island region thickened to more than 10 m, yet no prominent dispersion-driven upward cone formed in the island's core

area. Scale effects exert their influence primarily in two aspects: with increasing scale, the heterogeneity of the aquifer medium becomes more complex, which may mask the unique migration behavior of nanoplastics. Additionally, streamline curvature is reduced and flow velocity distributions are more homogeneous at larger scales, thereby reducing the influence of local streamline curvature on particle migration.

Upon pumping initiation at the field scale, the depth of the freshwater lens decreased from 20.168 m to 13.785 m, while the maximum depth of the freshwater lens encircled by nanoplastics decreased from 17.943 m to 14.610 m. Fig. 6(c_1-c_3) depicts variations in nanoplastic concentration within the lens: the volumetric fraction of nanoplastics occupying the freshwater lens decreased from 31.48% to 23.40%, a trend that deviates from the increasing pattern observed at the laboratory scale. Fig. 6(d_1-d_4) reveals the existence of a ~3 m-thick residual nanoplastic-bearing layer within the freshwater lens, with concentrations at 1-5% of the nanoplastic concentration in seawater. Upon stabilization of pumping, the transition zone migrated upward toward the lateral high-velocity discharge zones but no new upward cone was generated. At the field scale, the enhancement of nanoplastic dispersion relative to solute dispersion was no longer pronounced, a phenomenon likely due to improved flow stability and inherent scale effects. In addition, the residence time of colloidal filtration and entrainment processes is extended at this scale, which may consequently modify the final spatial distribution of nanoplastics.

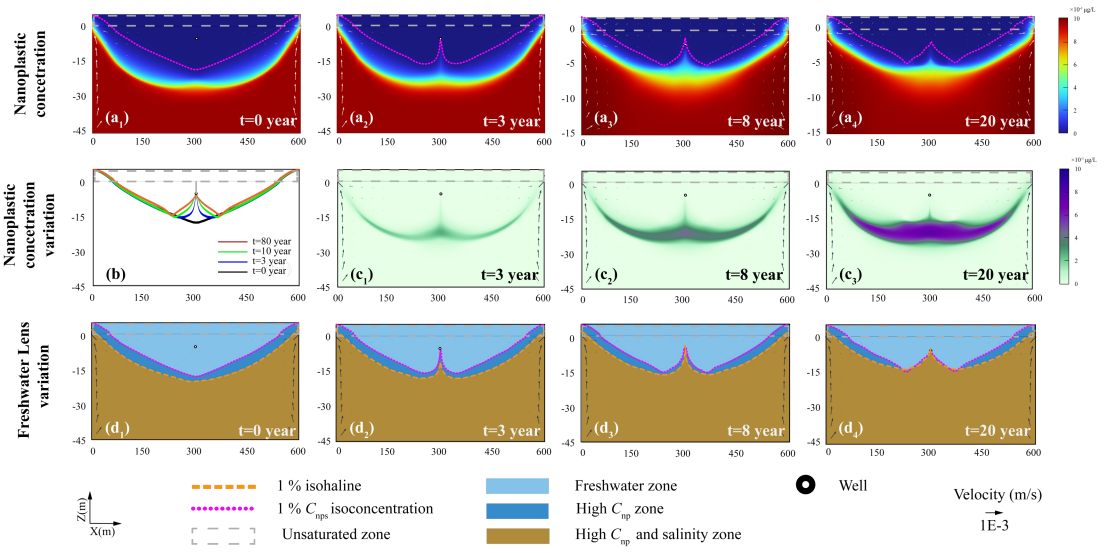

469

470 Fig. 6. Hydrophobic nanoplastic concentration dynamics and corresponding
471 freshwater lens alterations at field scale (600 m×50 m) during pumping (R_S = 51%) in
472 numerical simulations: (a_1-a_4) Freshwater lenses demarcated by the 1% PS-Pd-2
473 nanoplastic isoconcentration line at 0, 3, 8 and 20 years post-pumping; (b) 1% C_{nps}
474 isoconcentration line variation; (c_1-c_3) Net nanoplastic concentration variations
475 relative to the initial time point (0 year) at 3, 8 and 20 years post-pumping; (d_1-d_4)
476 Spatial offset between the 1% isohaline and 1% C_{nps} isoconcentration line around the
477 freshwater lens.

478 **3.3 Sensitivity Analysis**

479 Four factors were selected for analysis, with the *VR*, *ASYR*, and *RRSY* metrics
480 employed to evaluate nanoplastic contamination in freshwater and freshwater lenses,
481 as well as its implications for pumping operations.

482 Fig. 7(a_1, b_1) demonstrates that nanoplastic dispersivity exhibits a significant
483 correlation with *VR*, and nanoplastic dispersivity exerts a notable influence on
484 pumping efficiency. When nanoplastic dispersivity is lower than that of solutes, the
485 distribution range of nanoplastics closely approximates that of solutes, resulting in a
486 narrow transition zone, while Q_{Amax} is exclusively governed by salinity. When
487 nanoplastic dispersivity equals that of solutes, the nanoplastic-constrained freshwater
488 lens zone nearly overlaps with the salinity-defined freshwater lens zone. As

dispersivity increases to 10 times that of solutes, the volume of freshwater lenses decreases by approximately 30%. When the effective dispersivity of nanoplastics exceeds 17 times that of dissolved salts, the expanded dispersion range causes the 1% C_{nps} isoconcentration line to cover the wellhead area. The high sensitivity of nanoplastic behavior to dispersivity stems from their particulate nature: nanoplastics migrate not only via hydraulic dispersion but also through mechanisms such as Brownian motion, gravitational settling, and media interception. High dispersivity reflects the selective migration capacity of nanoplastics within complex pore structures, which is closely associated with their surface properties and hydrodynamic characteristics.

Fig. 7(a_2,b_2) reveals that *VR* gradually increases with rising hydraulic conductivity. At a hydraulic conductivity of 250 cm/min, 46.68% of the freshwater lens area is occupied by high-concentration nanoplastics. Under pumping conditions, both high hydraulic conductivity and high-permeability media result in a significant reduction in the usable portion of freshwater lens layers surrounded by nanoplastics. Aquifer hydraulic conductivity is another critical parameter regulating solute migration and retention. Previous studies have demonstrated that higher hydraulic conductivities result in reduced freshwater lens volumes and correspondingly decreased groundwater availability (Bailey and Jenson, 2014; Cui et al., 2021; Gao et al., 2025). The spatial distribution and magnitude of freshwater lenses surrounded by nanoplastics are consistent with these findings. High hydraulic conductivity accelerates freshwater discharge on both sides of the island, reducing the area where freshwater lenses can maintain equilibrium. For nanoplastics, increased hydraulic conductivity enhances flow velocity and convective transport capacity, thereby facilitating their intrusion into freshwater lenses.

Recharge rates were used to represent effective rainfall infiltration on the island. Fig. 7(a_3) shows that recharge significantly reduces the spatial distribution density of nanoplastics within freshwater lenses, with this effect being pronounced both before and after pumping. Increased recharge leads to a decrease in *VR*; when recharge rises

to 1.0 cm/min, *VR* declines to 33%. Conversely, when recharge drops below 0.65 cm/min, the final variation in *VR* also weakens, suggesting that nanoplastic concentrations are more difficult to mitigate with increased pumping intensity. Fig. 7(b_3) illustrates that enhanced recharge reduces the volume occupied by high-concentration nanoplastics in freshwater lenses, significantly increasing exploitable freshwater volume and alleviating the impact of nanoplastics on maximum safe pumping rates. Previous studies indicate that the volume and thickness of island freshwater lenses are positively correlated with precipitation (Zheng et al., 2025). The "flushing effect" of recharge on nanoplastic distribution likely operates through two mechanisms: first, recharge acts as the main source of freshwater storage in lenses. As the freshwater lens area expands, the thick transition zone formed by hydrophobic nanoplastics remains unaffected by convection and maintains a constant thickness, leading to a reduced proportion of nanoplastics despite unchanged total volume. Second, increased recharge may expand the strong convection zones on both sides of the seawater boundary, shrinking the central "stagnation zone" and thereby relatively weakening dispersion effects.

Among the analyzed media and environmental conditions, dispersivity emerges as the key parameter governing nanoplastic retention behavior in freshwater lenses, with high dispersivity exerting the most pronounced inhibitory effect on Q_{Amax}.

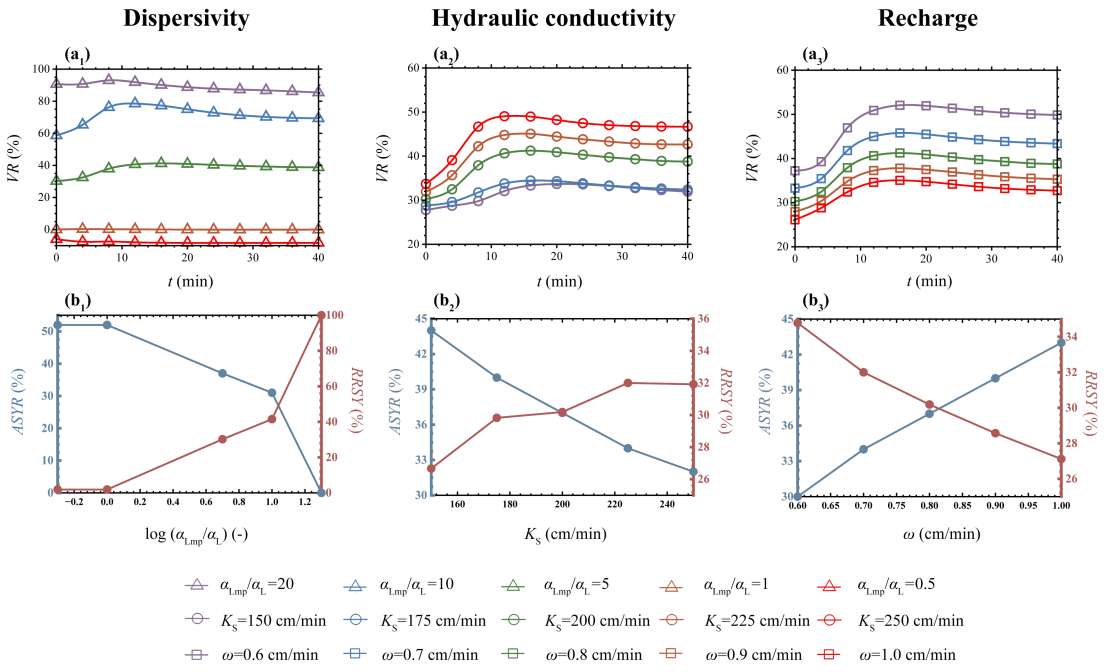

537

538 Fig. 7. The volume reduction rate of freshwater lenses (*VR*), the ratio of actual
539 maximum safe extraction capacity to theoretical maximum safe extraction capacity
540 (*ASYR*), and the ratio of maximum safe extraction capacity reduction due to
541 nanoplastic retention to maximum safe extraction capacity (*RRSY*) versus (a_1-a_3)
542 dispersivity, (b_1-b_3) hydraulic conductivity, and (c_1-c_3) recharge rate in numerical
543 simulations.

544 Fig. 8(a) and (b) present the theoretically derived maximum safe pumping rate
545 near the freshwater lens center (Tang et al., 2021) and the actual maximum safe
546 pumping rate, respectively. Under standard pumping conditions, the presence of a
547 transition zone reduces the effective area of the freshwater lens by 16.12% and its
548 thickness by 7.77 m. The position of pumping wells directly influences pumping rates:
549 as the distance from the central region increases, pumping rates decrease linearly, as
550 expressed in Equation (5). Simulation results demonstrate that the maximum safe
551 pumping rate of freshwater lenses does not exhibit a perfect linear correlation with the
552 distance from the surface central axis. During shallow pumping, higher rates may
553 even be achieved near the coastal sides due to the low-velocity zone in the center.
554 Under salinity-based constraints, the actual maximum safe pumped volume occurs at
555 the pumping point (x_m=20 cm, y=0 cm), corresponding to approximately two-thirds of

the half-width of the island from the central axis, with a pumping rate of 2.667×10^{-5} kg/s (200% of the theoretical value). At the center, the rate decreases to 2.480×10^{-5} kg/s, equivalent to 62% of the theoretical value. Under idealized strip-shaped island hydrodynamic conditions, seawater infiltrates from both bottom sides, forming an outflow zone at the top of the coastline, with a "stagnation zone" emerging in the island center—a phenomenon confirmed in previous studies. Owing to the slow, predominantly vertical flow in the central region, residual brackish water persists and disperses upward primarily via vertical dispersion. Thus, for single-well pumping projects on small idealized strip-shaped islands, central pumping may not be optimal, whereas lateral single-well operations can yield higher freshwater outputs. For deep pumping, given that freshwater lenses on such islands are approximately semicircular, deeper pumping is feasible near the center.

Fig. 8(c) illustrates that nanoplastic concentration constraints reduce freshwater lens volume by 13-28%, with more significant reductions in areas farther from the island's surface central axis, attributed to the uneven distribution of the nanoplastic transition zone. With respect to the reduction in maximum safe pumping rates, Fig. 8(d) demonstrates the decline in pumped volumes at the island center when nanoplastic concentration limits are considered. Centered at the pumping point (x_m=10 cm, y=0 cm), the maximum safe pumped volume gradually decreases with increasing distance from this center due to nanoplastic concentration restrictions. Near the seawater boundary, the transition zone completely covers the area within 10 cm of the shoreline. Under the 1% C_{nps} concentration limit, regions deeper than 25 mm are designated as non-exploitable zones. This phenomenon arises because the nanoplastic transition zone is relatively extended in the island's central region. Certain central regions exhibit pathway advantages, facilitating faster nanoplastic accumulation into wells. Near the seawater boundary, exploitable volumes decrease due to the influence of seawater nanoplastic source concentrations. Consequently, the combined effect of these two factors results in the highest exploitable volumes occurring in the upper regions near the central axis.

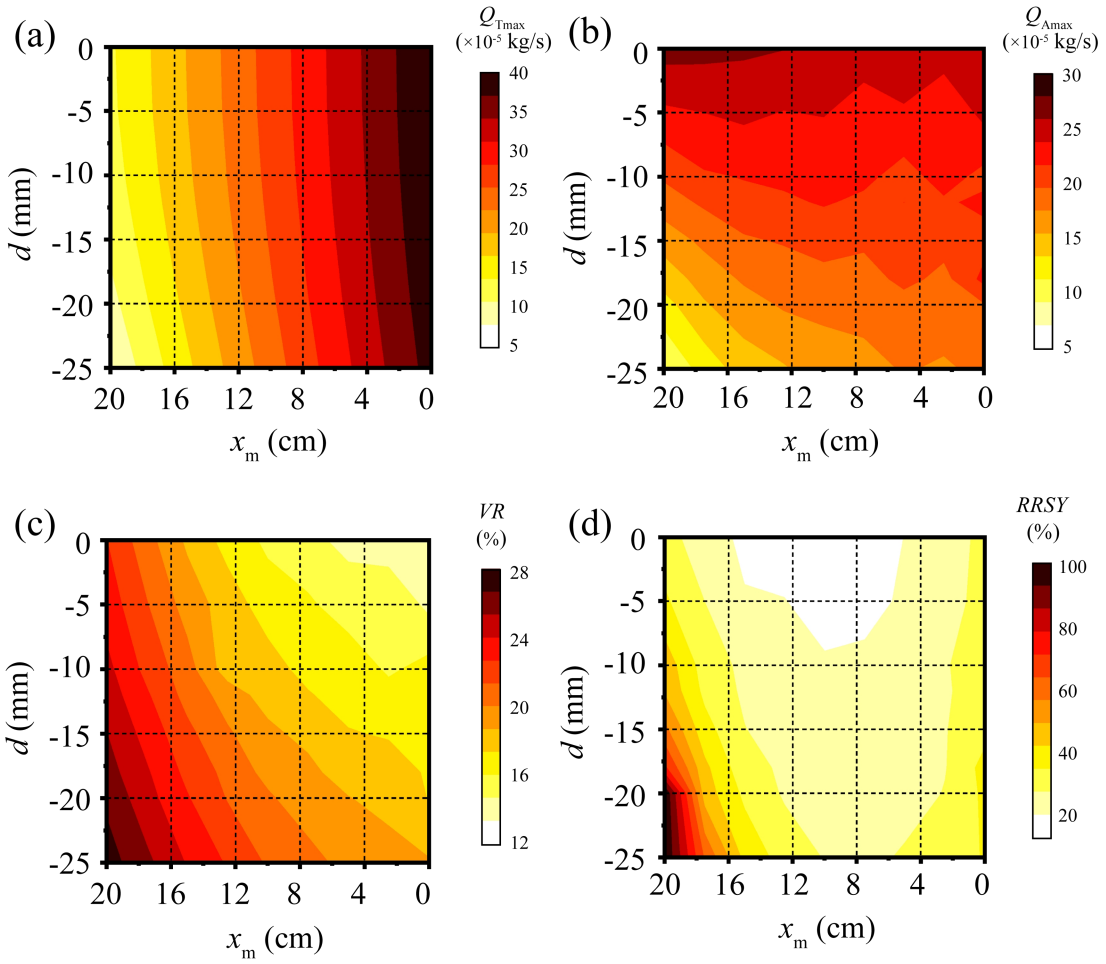

585

586 Fig. 8. Effects of pumping depth (d) and horizontal distance from the island center (x_m)
587 on (a) theoretical maximum safe extraction rate (Q_{Tmax}), (b) actual maximum safe
588 extraction rate (Q_{Amax}), (c) freshwater lens volume reduction rate (VR), and (d)
589 reduction ratio of safe yield caused by nanoplastic retention (RRSY) in the idealized
590 strip-island aquifer.

591

592 **4. Conclusion**

593 This study established a coupled variable-density groundwater flow and transport
594 model to explore nanoplastic migration in the freshwater lenses of idealized strip
595 islands under pumping scenarios. By integrating laboratory-calibrated parameters
596 with field-scale simulations, we identified fundamental differences between

nanoplastic and traditional solute transport processes and evaluated their implications for groundwater management in island aquifers. Key conclusions are summarized as follows:

(1) Nanoplastic transport differs fundamentally from dissolved salt transport within the freshwater lenses of idealized strip-island aquifers during groundwater pumping. In contrast to dissolved salts, whose behavior is mainly regulated by advection and dispersion, nanoplastics are further affected by particle-specific processes, such as adsorption-desorption, clogging, and filtration. The higher effective dispersivity leads to earlier breakthrough at extraction wells and the development of broader contaminant transition zones compared to salinity alone under pumping-induced upconing conditions in coastal island aquifers.

(2) Transport behavior exhibits strong scale dependence in strip-island freshwater lens systems under pumping stress. Laboratory-scale simulations showed rapid contamination and prominent "upper cone" formation within minutes, whereas field-scale simulations demonstrated attenuated upward coning and much longer stabilization times on the order of years. This contrast highlights the importance of multi-scale modeling when extrapolating experimental results to real-world island aquifers subject to freshwater extraction and seawater intrusion.

(3) Dispersivity is the dominant control on nanoplastic risk for pumping wells tapping freshwater lenses in strip-island coastal aquifers. Among the evaluated parameters, nanoplastic dispersivity exerts the strongest influence on contaminant accumulation in extraction wells, with hydraulic conductivity and recharge rates playing secondary but important roles. When nanoplastic dispersivity exceeds approximately 17 times that of dissolved solutes, the contaminant plume can fully envelop the well screen, reducing the maximum safe extraction rate to 37-50% of the salinity-based thresholds under island pumping scenarios.

(4) Well placement strategies must account for nanoplastic transition zones. Traditional guidelines based solely on salinity intrusion may not minimize

contamination risks. Simulations suggest that central pumping locations are not always optimal; lateral well placement can increase freshwater yield, although the optimal position depends on whether salinity or nanoplastic concentration is used as the limiting criterion.

Several simplifying assumptions were adopted in this study, including homogeneous aquifer properties, idealized boundary conditions, and limited representation of nanoplastic diversity. In practice, aquifer heterogeneity, tidal fluctuations and storm events may further influence the groundwater flow field and, consequently, the transport of substances. Furthermore, the diverse properties of environmental nanoplastics such as particle size distribution, aging state and surface chemistry will also bring additional impacts on their migration. In addition, only two types of synthetic nanoplastics were considered in this study, whereas natural systems contain a broader and more complex spectrum of particles. Despite these limitations, the present study establishes a mechanistic framework for evaluating nanoplastic transport in coastal freshwater lenses. By coupling variable-density flow with particle-specific transport processes and quantifying impacts on safe extraction thresholds, this study provides clear practical implications for well design, pumping optimization, and groundwater management on small islands. Future research should perform heterogeneous aquifer simulations, consider dynamic tidal and sea-level rise scenarios, and adopt more realistic natural micro/nanoplastic properties to further improve prediction accuracy and practical applicability for water security in plastic-polluted coastal environments.

Data availability

The data of this study can be found in Zheng (2026, https://zenodo.org/records/19150343).

Author contributions

TYZ: Conceptualization, Writing-Original Draft, Methodology, Resources, Writing-Review and Editing, Funding acquisition, Supervision.

CXM: Investigation, Software, Writing-Original Draft, Writing-Review and Editing, Visualization, Data Curation, Conceptualization.

SBG: Methodology, Formal Analysis, Investigation, Visualization, Writing-Review and Editing.

JL: Writing-Review and Editing, Methodology, Supervision, Conceptualization.

Competing interests

The contact author has declared that none of the authors has any competing interests.

Financial support

This work was supported by the National Natural Science Foundation of China (No. 42422207), Taishan Scholars Program of Shandong Province (No. tsqn202408078) and the Postdoctoral Fellowship Program of CPSF under Grant Number GZC20250290.

References

Abdoulhalik, A., and Ahmed, A. A.: Transient investigation of saltwater upconing in laboratory-scale coastal aquifer, Estuarine, Coastal and Shelf Science, 214, 149-160, https://doi.org/10.1016/j.ecss.2018.09.024, 2018.

Al Harraq, A., and Bharti, B.: Microplastics through the Lens of Colloid Science, ACS Environmental Au, 2(1), 3-10, https://doi.org/10.1021/acsenvironau.1c00016, 2022.

Alkindi, A., Al-Wahaibi, Y., Bijeljic, B. and Muggeridge, A.: Investigation of longitudinal and transverse dispersion in stable displacements with a high viscosity and density contrast between the fluids. Journal of Contaminant Hydrology, 120-121, 170-183, https://doi.org/10.1016/j.jconhyd.2010.06.006, 2011.

Alsumaiei, A. A., and Bailey, R. T.: Quantifying threats to groundwater resources in the Republic of Maldives Part I: Future rainfall patterns and sea-level rise, Hydrological Processes, 32(9), 1137-1153, https://doi.org/10.1002/hyp.11480, 2018.

Amirmoshiri, M., Zhang, L., Puerto, M. C., Tewari, R. D., Bahrim, R. Z. B. K., Farajzadeh, R., Hirasaki, G. J., and Biswal, S. L.: Role of Wettability on the Adsorption of an Anionic Surfactant on Sandstone Cores, Langmuir, 36(36), 10725-10738, https://doi.org/10.1021/acs.langmuir.0c01521, 2020.

Babakhani, P., Bridge, J., Doong, R. A., and Phenrat, T.: Continuum-based models and concepts for the transport of nanoparticles in saturated porous media: A state-of-the-science review, Advances in colloid and interface science, 246, 75-104, https://doi.org/10.1016/j.cis.2017.06.002, 2017.

Babu, R., Park, N., and Nam, B.: Regional and well-scale indicators for assessing the sustainability of small island fresh groundwater lenses under future climate conditions, Environmental Earth Sciences, 79(1), 47, https://doi.org/10.1007/s12665-019-8773-3, 2020.

Bailey, R. T., and Jenson, J. W.: Effects of Marine Overwash for Atoll Aquifers: Environmental and Human Factors, Groundwater, 52(5), 694-704, https://doi.org/10.1111/gwat.12117, 2014.

Chen, G., Zou, Y., Xiong, G., Wang, Y., Zhao, W., Xu, X., Zhu, X., Wu, J., Song, F., and Yu, H.: Microplastic transport and ecological risk in coastal intruded aquifers based on a coupled seawater intrusion and microplastic risk assessment model, Journal of hazardous materials, 480, 135996, https://doi.org/10.1016/j.jhazmat.2024.135996, 2024.

Chen, Q., Zhang, L., Shen, C., and Lu, C.: Effects of groundwater pumping on pore water flow and salt transport in tide-controlled unconfined coastal aquifers, Hydrological Processes, 38(8), e15261, https://doi.org/10.1002/hyp.15261, 2024a.

Coulon, C., Lemieux, J. M., Pryet, A., Bayer,P., Young, N. L., and Molson, J.: Pumping Optimization Under Uncertainty in an Island Freshwater Lens Using a Sharp-Interface Seawater Intrusion Model, Water Resources Research, 58(8), e2021WR031793, https://doi.org/10.1029/2021WR031793, 2022.

Cui, X., Zhu, C., Hu, M., Wang, R., and Liu, H.: Permeability of porous media in coral reefs, Bulletin of Engineering Geology and the Environment, 80(6), 5111-5126, https://doi.org/10.1007/s10064-020-02082-5, 2021.

Dagan, G., and Bear, J.: Solving The Problem Of Local Interface Upconing In A Coastal Aquifer By The Method Of Small Perturbations, Journal of Hydraulic Research, 6(1), 15-44, https://doi.org/10.1080/00221686809500218, 1968.

Dose, E. J., Stoeckl, L., Houben, G. J., Vacher, H. L., Vassolo, S., Dietrich, J., and Himmelsbach, T.: Experiments and Modeling of Freshwater Lenses in Layered Aquifers: Steady State Interface Geometry, Journal of Hydrology, 509, 621-630, http://dx.doi.org/10.1016/j.jhydrol.2013.10.010, 2014.

Gao, C., Zheng, T., Chang, Q., Zheng, X., Song, X., and Luo, J.: Dynamics of Irregular Freshwater Lenses Evolution in Thin Aquifers of Reclaimed Circular Islands, Water Resources Research, 61(7), e2024WR038880, https://doi.org/10.1029/2024WR038880, 2025.

Gelhar, L. W., Welty, C., and Rehfeldt, K. R.: A critical review of data on field-scale dispersion in aquifers, Water Resources Research, 28(7), 1955-1974, https://doi.org/10.1029/92WR00607, 1992.

Gonçalves, J. M., and Bebianno, M. J.: Nanoplastics impact on marine biota: A review. Environmental Pollution, 273, 116426, https://doi.org/10.1016/j.envpol.2021.116426, 2021.

Houben, G., and Post, V. E. A.: The first field-based descriptions of pumping-induced saltwater intrusion and upconing, Hydrogeology Journal, 25(1), 243-247, https://doi.org/10.1007/s10040-016-1476-x, 2017.

Isobe, A., Iwasaki, S., Uchida, K., and Tokai, T.: Abundance of non-conservative microplastics in the upper ocean from 1957 to 2066, Nature Communications, 10(1), 417, https://doi.org/10.1038/s41467-019-08316-9, 2019.

Johnson, W. P.: Quantitative Linking of Nanoscale Interactions to Continuum-Scale Nanoparticle and Microplastic Transport in Environmental Granular Media, Environmental Science & Technology, 54(13), 8032-8042, https://doi.org/10.1021/acs.est.0c01172, 2020.

Ketabchi, H., Mahmoodzadeh, D., Ataie-Ashtiani, B., Werner, A. D., and Simmons, C. T.: Sea-level rise impact on fresh groundwater lenses in two-layer small islands, Hydrological Processes, 28(24), 5938-5953, https://doi.org/10.1002/hyp.10059, 2014.

Koelmans, A. A., Redondo-Hasselerharm, P. E., Nor, N. H. M., de Ruijter, V. N., Mintenig, S. M., and Kooi, M.: Risk assessment of microplastic particles, Nature Reviews Materials, 7(2), 138-152, https://doi.org/10.1038/s41578-021-00411-y, 2022.

Koutnik, V. S., Leonard, J., Alkidim, S., DePrima, F. J., Ravi, S., Hoek, E. M. V., and Mohanty, S. K.: Distribution of microplastics in soil and freshwater environments: Global analysis and framework for transport modeling, Environmental pollution (Barking, Essex : 1987), 274, 116552, https://doi.org/10.1016/j.envpol.2021.116552, 2021.

Lee, J., Rolle, M. and Kitanidis, P.: Longitudinal dispersion coefficients for numerical modeling of groundwater solute transport in heterogeneous formations, Journal of Contaminant Hydrology, 212, 41-54, https://doi.org/10.1016/j.jconhyd.2017.09.004, 2017.

Li, J., Liu, H., and Paul Chen, J.: Microplastics in freshwater systems: A review on occurrence, environmental effects, and methods for microplastics detection, Water Research, 137, 362-374, https://doi.org/10.1016/j.watres.2017.12.056, 2018.

Li, M., Zhang, M., Rong, H., Zhang, X., He, L., Han, P., and Tong, M.: Transport and deposition of plastic particles in porous media during seawater intrusion and groundwater-seawater displacement processes, Science of The Total Environment, 781, 146752, https://doi.org/10.1016/j.scitotenv.2021.146752, 2021.

Liu, X., Zhao, R., Liu, M., Zheng, T., Hao, Y., Wang, C., Liu, L., Zhao, Y., Liu, Z., Dai, Y., Yue, T., Zhao, J., Wang, Z., and Xing, B.: Transport of eco-corona coated nanoplastics in coastal sediments, Water research, 284, 123893, https://doi.org/10.1016/j.watres.2025.123893, 2025.

753 Muskat, M.: The flow of homogeneous fluids through porous media, Soil Sci, 46(2), 169,
754 https://journals.lww.com/soilsci/fulltext/1938/08000/the_flow_of_homogeneous_fluids_throu
755 gh_porous.8.aspx, 1938.
756 Ranjan, V. P., Joseph, A., Sharma, H. B., and Goel, S.: Preliminary investigation on effects of size,
757 polymer type, and surface behaviour on the vertical mobility of microplastics in a porous
758 media, Science of The Total Environment, 864, 161148,
759 https://doi.org/10.1016/j.scitotenv.2022.161148, 2023.
760 Ren, Z., Gui, X., Xu, X., Zhao, L., Qiu, H., and Cao, X.: Microplastics in the soil-groundwater
761 environment: Aging, migration, and co-transport of contaminants - A critical review, Journal
762 of hazardous materials, 419, 126455, https://doi.org/10.1016/j.jhazmat.2021.126455, 2021.
763 Ren, Z., Gui, X., Xu, X., Zhao, L., Qiu, H., Wang, X., and Cao, X.: Weathering of microplastics
764 and their enhancement on the retention of cadmium in coastal soil saturated with seawater,
765 Journal of hazardous materials, 440, 129850, https://doi.org/10.1016/j.jhazmat.2022.129850,
766 2022.
767 Sayre, R., Noble, S., Hamann, S., Smith, R., Wright, D., Breyer, S., Butler, K., Van Graafeiland,
768 K., Frye, C., Karagulle, D., Hopkins, D., Stephens, D., Kelly, K., Basher, Z., Burton, D.,
769 Cress, J., Atkins, K., Van Sistine, D. P., Friesen, B., Allee, R., Allen, T., Aniello, P., Asaad, I.,
770 Costello, M. J., Goodin, K., Harris, P., Kavanaugh, M., Lillis, H., Manca, E., Muller-Karger,
771 F., Nyberg, B., Parsons, R., Saarinen, J., Steiner, J., and Reed, A.: A new 30 meter resolution
772 global shoreline vector and associated global islands database for the development of
773 standardized ecological coastal units, Journal of Operational Oceanography, 12(sup2),
774 S47-S56, https://doi.org/10.1080/1755876X.2018.1529714, 2019.
775 Sharan, A., Lal, A., and Datta, B.: A review of groundwater sustainability crisis in the Pacific
776 Island countries: Challenges and solutions, Journal of Hydrology, 603, 127165,
777 https://doi.org/10.1016/j.jhydrol.2021.127165., 2021.
778 Singh, A., Chauhan, A., and Gaur, R.: A comprehensive review on the synthesis, properties,
779 environmental impacts, and chemiluminescence applications of polystyrene (PS), Discover
780 Chemistry, 2(1), 47, https://doi.org/10.1007/s44371-025-00125-y, 2025.
781 Stoeckl, L., and Houben, G.: Flow dynamics and age stratification of freshwater lenses:
782 Experiments and modeling, Journal of Hydrology, 458-459, 9-15,
783 https://doi.org/10.1016/j.jhydrol.2012.05.070., 2012.
784 Tang, Y., Lu, C., and Luo, J.: An Analytical solution for groundwater lens pumping in a
785 three-dimensional rectangular island, Journal of Hydrology, 617, 128928,
786 https://doi.org/10.1016/j.jhydrol.2022.128928, 2022.
787 Tang, Y., Lu, C., and Luo, J.: Optimizing groundwater pumping in small island groundwater lenses:
788 An analytical approach, Journal of Hydrology, 629, 130579,
789 https://doi.org/10.1016/j.jhydrol.2023.130579, 2024.
790 Tang, Y., Rathore, S., Lu, C., and Luo, J.: Development of Groundwater Lens for Transient
791 Recharge in Strip Islands, Journal of Hydrology, 590, 125209,
792 https://doi.org/10.1016/j.jhydrol.2020.125209, 2020.
793 Tang, Y., Yan, M., Wang, X., Lu, C., and Luo, J.: Experimental and modeling investigation of
794 pumping from a fresh groundwater lens in an idealized strip island, Journal of Hydrology,
795 602, 126734, https://doi.org/10.1016/j.jhydrol.2021.126734, 2021.
796 ten Hietbrink, S., Materić, D., Holzinger, R., Groeskamp, S., and Niemann, H.: Nanoplastic

797 concentrations across the North Atlantic, Nature, 643(8071), 412-416,
798 https://doi.org/10.1038/s41586-025-09218-1, 2025.
799 Thompson, R. C., Courtene-Jones, W., Boucher, J., Pahl, S., Raubenheimer, K., and Koelmans, A.
800 A.: Twenty years of microplastic pollution research—what have we learned?, Science,
801 386(6720), eadl2746, https://doi.org/10.1126/science.adl2746, 2024.
802 van Genuchten, M.T.: A Closed-form Equation for Predicting the Hydraulic Conductivity of
803 Unsaturated Soils, Soil Science Society of America Journal, 44: 892-898,
804 https://doi.org/10.2136/sssaj1980.03615995004400050002x, 1980.
805 Voss, C., and Provost, A. M.: SUTRA: A model for 2D or 3D saturated-unsaturated,
806 variable-density ground-water flow with solute or energy transport, Report Rep. 2002-4231,
807 https://doi.org/10.3133/wri024231, 2002.
808 Waldschläger, K., and Schüttrumpf, H.: Infiltration Behavior of Microplastic Particles with
809 Different Densities, Sizes, and Shapes—From Glass Spheres to Natural Sediments,
810 Environmental Science & Technology, 54(15), 9366-9373,
811 https://doi.org/10.1021/acs.est.0c01722, 2020.
812 Wang, R., Shu, L., Zhang, R., and Ling, Z.: Determination of Exploitable Coefficient of Coral
813 Island Freshwater Lens Considering the Integrated Effects of Lens Growth and Contraction,
814 Water, 15(5), 890, https://doi.org/10.3390/w15050890, 2023.
815 Wang, X., Bolan, N., Tsang, D. C. W., Sarkar, B., Bradney, L., and Li, Y.: A review of
816 microplastics aggregation in aquatic environment: Influence factors, analytical methods, and
817 environmental implications, Journal of hazardous materials, 402, 123496,
818 https://doi.org/10.1016/j.jhazmat.2020.123496, 2021.
819 Wang, Z., and Sedighi, M.: Dispersion properties of nanoplastic spheres in granular media at low
820 Reynolds numbers, Journal of Contaminant Hydrology, 259, 104244,
821 https://doi.org/10.1016/j.jconhyd.2023.104244, 2023.
822 Werner, A. D., Jakovovic, D., and Simmons, C. T.: Experimental observations of saltwater
823 up-coning, Journal of Hydrology, 373(1), 230-241,
824 https://doi.org/10.1016/j.jhydrol.2009.05.004, 2009.
825 White, I., and Falkland, T.: Management of freshwater lenses on small Pacific islands,
826 Hydrogeology Journal, 18(1), 227-246, https://doi.org/10.1007/s10040-009-0525-0, 2010.
827 Yan, M., Lu, C., Werner, A. D., and Luo, J.: Analytical, Experimental, and Numerical
828 Investigation of Partially Penetrating Barriers for Expanding Island Freshwater Lenses, Water
829 Resources Research, 57(3), e2020WR028386, https://doi.org/10.1029/2020WR028386, 2021.
830 Yang, J., Wang, Q., Heidbüchel, I., Xu, T., and Lu, C.: Cut-off walls alter nitrogen loads and fluxes
831 in small islands, Journal of Hydrology, 647, 132266,
832 https://doi.org/10.1016/j.jhydrol.2024.132266, 2025.
833 Yao, Y., Andrews, C., Zheng, Y., He, X., Babovic, V., and Zheng, C.: Development of Fresh
834 Groundwater Lens in Coastal Reclaimed Islands, Journal of Hydrology, 573, 365-375,
835 https://doi.org/10.1016/j.jhydrol.2019.03.062, 2019.
836 Yuan, C., Hu, L., Ren, Z., Xu, X., Gui, X., Gong, X., Wu, R., Sima, J., and Cao, X.: Marine
837 Microplastics Enhance Release of Arsenic in Coastal Aquifer during Seawater Intrusion
838 Process, Journal of Hazardous Materials, 475, 134804,
839 https://doi.org/10.1016/j.jhazmat.2024.134804, 2024.
840 Zheng, T. (2014), Numerical Analysis of Modeling Concepts for Salt Precipitation and Porosity -

Permeability Evolution during Brine Evaporation, M.Eng. thesis, University of Stuttgart, 2014.

Zheng, T., Meng, Y., Meng, X., Gao, S., Zhang, L., Zhang, B., Liu, T., and Luo, J.: Influence of time-space variability of rainfall infiltration recharge on fresh groundwater lens, Physics of Fluids, 37(3), 036623, https://doi.org/10.1063/5.0253940, 2025.